From stripe to checkerboard ordering of charge-density waves on the square lattice in the presence of quenched disorder

Adrian Del Maestro, Bernd Rosenow,* and Subir Sachdev
Department of Physics, Harvard University, Cambridge, Massachusetts 02138, USA
(Received 1 March 2006; revised manuscript received 1 May 2006; published 25 July 2006)

We discuss the effects of quenched disorder on a model of charge density wave (CDW) ordering on the square lattice. Our model may be applicable to the cuprate superconductors, where a random electrostatic potential exists in the CuO_2 planes as a result of the presence of charged dopants. We argue that the presence of a random potential can affect the unidirectionality of the CDW order, characterized by an Ising order parameter. Coupling to a unidirectional CDW, the random potential can lead to the formation of domains with 90° relative orientation, thus tending to restore the rotational symmetry of the underlying lattice. We find that the correlation length of the Ising order can be significantly larger than the CDW correlation length. For a checkerboard CDW on the other hand, disorder generates spatial anisotropies on short length scales and, thus, some degree of unidirectionality. We quantify these disorder effects and suggest techniques for analyzing the spatially dependent local density of states data measured in scanning tunneling microscopy experiments.

DOI: 10.1103/PhysRevB.74.024520 PACS number(s): 74.20.De, 71.45.Lr, 74.62.Dh, 74.72.−h

I. INTRODUCTION

One of the major stumbling blocks preventing a quantitative confrontation between theory and experiment in the cuprate superconductors is the influence of quenched disorder on the experimental observations. The dopant ions exert a significant electrostatic potential on the CuO_2 plane, and thus, unless the ions can be carefully arranged in a regular pattern, the mobile charge carriers experience a random potential. Recent scanning tunneling microscopy (STM) observations[1–5] clearly display that quenched randomness is crucial in determining the spatial modulations of the local density of states (LDOS).

There has been much recent interest in determining the nature of the spin and charge density wave (CDW) order observed in STM, neutron, and x-ray scattering in a variety of cuprate compounds at low temperatures.[1–9] The quenched disorder acts on the CDW order as a "random field," which is always a relevant perturbation at low temperatures: true long-range order is disrupted at any finite random field strength.[10] Nevertheless, one might hope that an analytic treatment may be possible in the limit of weak random fields. Many such analyses[10–14] have been carried out in the literature, describing states with power-law correlations and suppressed dislocations (or related topological defects) at intermediate length scales. At the longest scales, dislocations always proliferate and all correlations are expected to decay exponentially; no analytic treatment is possible in this strong coupling regime. As we will discuss below, current experiments on the cuprates are in a regime dominated by dislocations, and there does not appear to be any significant regime of applicability of the defect-free theory. Consequently, we are forced to rely on numerical simulations for an understanding of experiments. We will present numerical results over a representative range of parameters. Our aim is to allow insights into the underlying theory by a comparison of experimental and numerical results.

II. MODEL

A previous work by two of the authors[15] studied the influence of thermal fluctuations on density wave order on the square lattice. Here, we study the influence of quenched randomness on the same underlying theory. A generic density was defined that could be any observable invariant under spin rotations and time reversal

$$\delta\rho(\boldsymbol{r}) = \mathrm{Re}[\Phi_x e^{i\boldsymbol{K}_x\cdot\boldsymbol{r}}] + \mathrm{Re}[\Phi_y e^{i\boldsymbol{K}_y\cdot\boldsymbol{r}}], \tag{2.1}$$

where $\boldsymbol{K}_x=(2\pi/a)(1/p,0)$, $\boldsymbol{K}_y=(2\pi/a)(0,1/p)$, a is the lattice spacing, and p is an integer describing the period of the CDW. $\Phi_{x,y}$ are complex order parameters, which were assumed to vary slowly on the scale of a lattice spacing.

If both amplitudes $|\Phi_{x,y}|$ have nonzero expectation values, the charge density is modulated in both x and y directions and describes a solid on the square lattice. In addition, if the wave length of the charge ordering is commensurate with the underlying crystal, i.e., for integer p, the density displays true long-range order. For incommensurate charge order, fluctuations due to finite temperature will cause quasi-long-range order with a power-law decay of correlation functions. If only one of the two amplitudes $|\Phi_{x,y}|$ has nonzero expectation value, the density Eq. (2.1) describes unidirectional (striped) CDW order. Again, the presence of a commensurate lattice potential makes the order long ranged at finite temperatures, whereas in the incommensurate case it is quasi long ranged.

In the incommensurate phase, in the absence of disorder, the free energy expanded in powers of $\Phi_{x,y}$ and its gradients consistent with the symmetries of the square lattice is given by

$$\mathcal{F}_\Phi = \int d^2r \Big[C_1(|\partial_x\Phi_x|^2 + |\partial_y\Phi_y|^2) + C_2(|\partial_y\Phi_x|^2 + |\partial_x\Phi_y|^2) + s(|\Phi_x|^2 + |\Phi_y|^2) + \frac{u}{2}(|\Phi_x|^2 + |\Phi_y|^2)^2 + v|\Phi_x|^2|\Phi_y|^2 \Big]. \tag{2.2}$$

The homogeneous mean field solution of this model is summarized in Fig. 1, where the checkerboard, stripe, and liquid

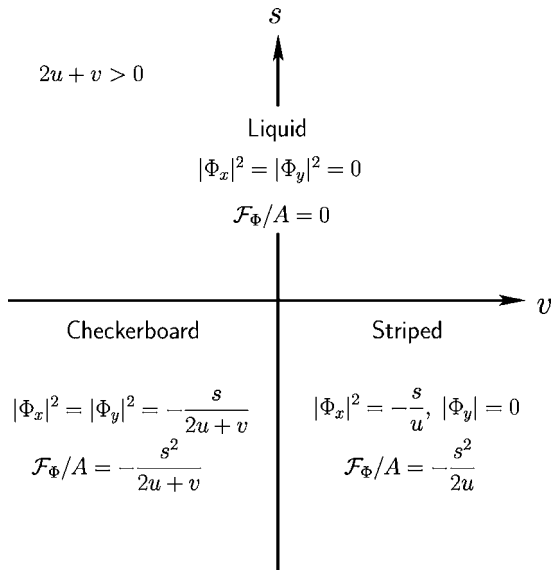

FIG. 1. The homogeneous mean field solutions of Eq. (2.2) for $\Phi_{x,y}$.

phase values of $\Phi_{x,y}$ are shown along with the accompanying free energy densities.

In this work we focus on the influence of quenched disorder on CDW order and thus consider adding a term to the free energy consisting of two complex random fields, coupling directly to $\Phi_{x,y}$

$$\mathcal{F}_{\mathrm{H}} = -\int d^2r(\mathrm{H}_x^*\Phi_x + \mathrm{H}_y^*\Phi_y + \mathrm{c.c.}), \tag{2.3}$$

resulting in the total action

$$\mathcal{F} = \mathcal{F}_\Phi + \mathcal{F}_{\mathrm{H}}, \tag{2.4}$$

where the complex random fields H_μ ($\mu = x,y$) are parametrized as $\mathrm{H}_\mu(\boldsymbol{r}) = h_\mu(\boldsymbol{r})e^{i\eta_\mu(r)}$, h_μ are Gaussian-distributed random variables with mean 0, and standard deviation h_0, and η_μ are uniformly distributed random phases on $[0,2\pi)$.

Let us confine ourselves to the condensed phase where $s < 0$, and $u > 0$ for stability. The interesting physics are encapsulated by the effects of altering the coupling constant v and the strength of the random field h_0. While v changes the low energy ground states from checkerboardlike configurations for $v < 0$ ($|\Phi_x| = |\Phi_y|$) to stripelike patterns ($|\Phi_\mu| \neq |\Phi_\nu| = 0$) for $v > 0$, h_0 should destabilize both types of states.

A careful treatment of the coupling between CDW order and a random electrostatic potential yields random compression terms of the form[14] $h_\mu \partial\Theta_\mu$ ($\Theta_\mu = \arg[\Phi_\mu]$) omitted in the free energy Eq. (2.3). In addition, an renormalization group analysis of the full action $\mathcal{F}_\Phi + \mathcal{F}_{\mathrm{H}}$ generates random shear terms. Random compression and shear terms are responsible for the power-law decay of correlation functions on intermediate length scales, on which the influence of topological excitations (dislocations) in the phase fields Θ_μ can be neglected.[14]

In STM experiments, the correlation length of charge order is found to have values ranging from[1] 2.5 to roughly[3] 5 CDW periods. In neutron scattering experiments, peak widths corresponding to correlation lengths larger than ten CDW periods were observed.[6,7] The correlation length describes the scale on which dislocations proliferate, and the presence of a relatively short correlation length indicates that there is no intermediate length scale on which compression and shear terms are important. For this reason, the omission of these terms from the elastic energy should be justified.

Although there is no explicit reference to the level of doping in the free energy equation (2.2), it can have several effects. It will directly influence the wave vector of CDW order, with higher doping levels corresponding to larger wave vectors. The doping level can also influence the energetics of CDW formation and, hence, the elastic constants in the free energy. As these elastic constants are effective parameters and should be determined from the analysis of experimental data, their dependence on the doping level need not be taken into account when analyzing the model. There may also be commensurability effects for doping levels near 1/8. Neglecting the influence of a random potential, changing the doping level in the presence of a periodic lattice potential gives rise to a commensurate-incommensurate transition.[15] In the presence of disorder, however, commensurability effects are manifest only as a crossover and not a phase transition, as the commensurate phase is unstable with respect to disorder-induced dislocations on large length scales.[16] Guided by the experimental results discussed above, in this study we are interested in the strong disorder regime with proliferating dislocations and thus commensurability effects are not important for our analysis.

III. NUMERICAL MINIMIZATION

Because of the presence of the two complex random fields $\mathrm{H}_\mu(\boldsymbol{r})$, we have elected to minimize Eq. (2.4) numerically. The interplay of elastic and disorder energy causes frustration and gives rise to an exponentially large number of low-lying states with similar energies but very different configurations. As these states are separated by large energy barriers, relaxation after an external perturbation is very slow and glassy dynamics can be observed. For these reasons, numerically finding the ground state of such a system is a hard problem and as novel algorithms are developed and employed, even to relatively simple models, new states with lower energies are inevitably found.[17]

Gradient methods that move strictly downhill in the energy landscape are fast, but prone to becoming stuck in local minima and are not always able to reproduce the results of slower ergodic methods. Simulated annealing algorithms[18] have been the most successful at thoroughly sampling the possible configuration space by using a fictitious temperature. By successively lowering this temperature, the resolution of finer and finer energy scales becomes possible while avoiding the danger of being stuck in a metastable excited state.

As a compromise, we have elected to employ a combination of both greedy conjugate gradient[19] and ergodic simulated annealing[20] methods. We allow for the possibility of local uphill moves where the configuration update involves

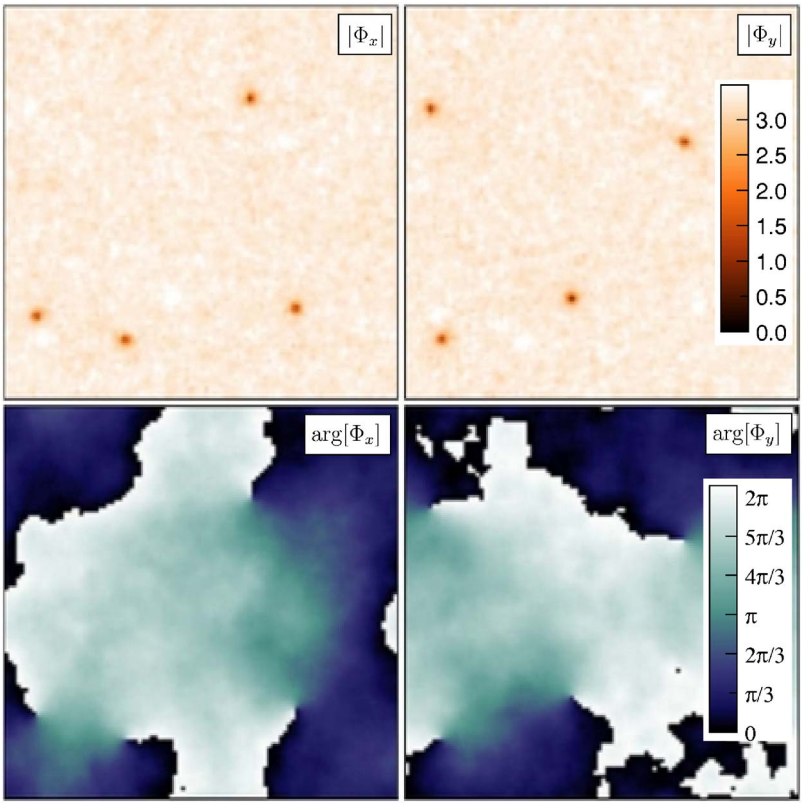

FIG. 2. (Color online) The ground state field configuration on a 100×100 lattice for a random field standard deviation of $h_0=0.6$ and xy interaction $v=-0.1$ for a particular realization of disorder.

making a downhill step in a random area of the sample. The size of the randomly chosen region is annealed by tracking metropolis acceptance rate. This method faithfully reproduces the results of early Monte Carlo work on the random field XY model.[21]

We have performed simulations for a number of lattice sizes $L=\{20,32,48,64,100\}$, commensurate with the experimentally observed[1–4] period of modulations in the local density of states of four lattice spacings ($p=4$) and multiple realizations of disorder $N_{rd}(L)=\{200,200,150,150,100\}$. Let us consider a $L\times L$ square lattice of N sites labeled by i, then after rescaling to give dimensionless coupling parameters, the continuum free energy of Eq. (2.4) in units where the lattice constant a is set to unity takes the form (with $\Theta_{\mu,i}=\arg[\Phi_{\mu,i}]$)

$$\mathcal{F}_L=-\frac{1}{2}\sum_{\mu=x,y}\sum_{\langle i,j\rangle}J_{\mu,j}|\Phi_{\mu,i}||\Phi_{\mu,j}|\cos(\Theta_{\mu,i}-\Theta_{\mu,j})+\sum_{\mu=x,y}\sum_{i}\left[(C_1+C_2+s)|\Phi_{\mu,i}|^2+\frac{u}{2}|\Phi_{\mu,i}|^4-2h_{\mu,i}|\Phi_{\mu,i}|\cos(\Theta_{\mu,i}-\eta_{\mu,i})\right]+(u+v)\sum_i|\Phi_{x,i}|^2|\Phi_{y,i}|^2, \tag{3.1}$$

with $\langle i,j\rangle$ indicating the usual sum over nearest neighbors and the factor of $1/2$ is inserted to avoid double counting. The coupling matrix $J_{\mu,j}$ has diagonal elements $J_{x,i\pm x}=J_{y,i\pm y}=C_1$ and off diagonal couplings $J_{x,i\pm y}=J_{y,i\pm x}=C_2$. We have chosen to set $C_1=C_2=1$ and $s=-0.1$, thus restoring full rotational symmetry of the elastic energy on scales much larger than the lattice spacing and confining our analysis to the condensed phase. We have also elected to pick the value of the quartic coupling u to ensure the condensation energy remains constant across the critical line $v=0$ by setting $u(v\geqslant 0)=-s$ and $u(v<0)=-(s+v/2)$.

IV. RESULTS

Employing this minimization procedure, we obtain stable low-energy field configurations, such as the ones shown in Figs. 2–4. For $v=-0.1$ and $h_0=0.6$ (Fig. 2), we observe small circular regions, <5 lattice spacings across, where the local random field configuration has taken a value that makes it energetically favorable to suppress the magnitude of either Φ_x or Φ_y in its vicinity. For the uncoupled theory (Fig. 3), $\Phi_{x,y}$ appear much smoother and although there still exists separate regions of stripe and checkerboard order, the interfaces between these regions are poorly defined. We may also observe the effects of positive $v=0.1$ at the same disorder strength as seen in Fig. 4. In this case, the magnitude of either Φ_x or Φ_y is suppressed to zero over large regions of the sample leading to a ground state field configuration with well-defined domains having unidirectional order in either the x or y directions.

We can construct the form of the density fluctuations $\delta\rho(\boldsymbol{r})$ [Eq. (2.1)] from the minimized value of the spatially dependent order parameters $\Phi_{x,y}(\boldsymbol{r})$ for CDWs with a period of four lattice spacings ($p=4$). We may then compare the results of $\delta\rho(\boldsymbol{r})$, seen in Fig. 5, for various values of v and h_0 to the STM experiments mentioned in Sec. I in an attempt to

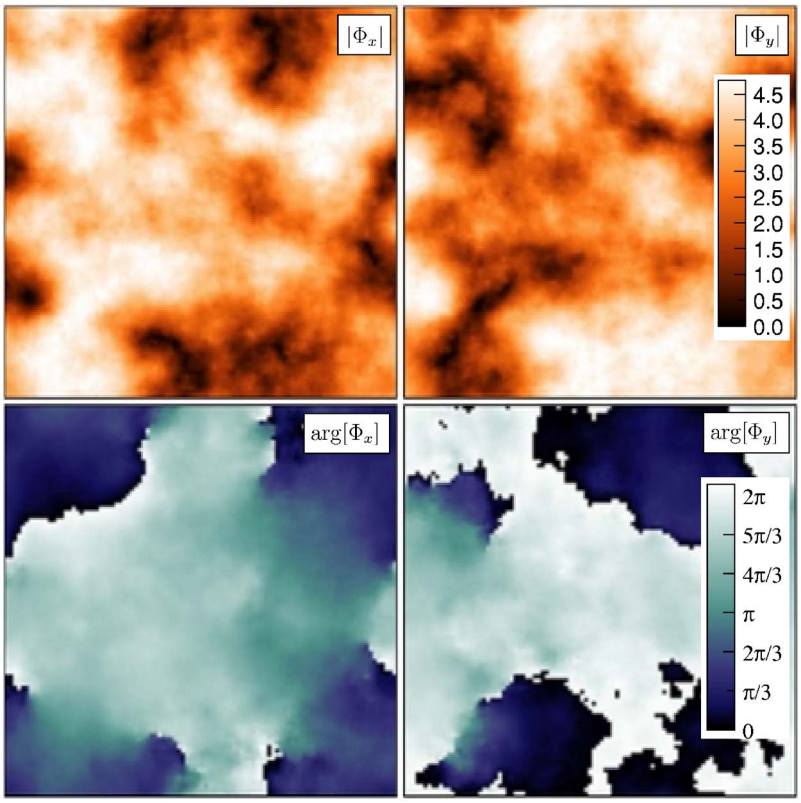

FIG. 3. (Color online) The ground state field configuration on a 100×100 lattice for a random field standard deviation of $h_0=0.6$ and xy interaction $v=0.0$ for a particular realization of disorder.

qualitatively identify the range of parameters in Eq. (2.4) corresponding to these experimental systems. For $v<0$ and $h_0=0.0$, we observe robust checkerboard ordering, which is coherent over the entire lattice. As the variance of the random field is increased, dislocations in the phase of the Φ_μ fields gradually destroy the local ordering, and the correlation length is reduced to less than three CDW periods for $h_0=1.2$. For $v=0.0$ and $h_0=0.0$, density fluctuations in the

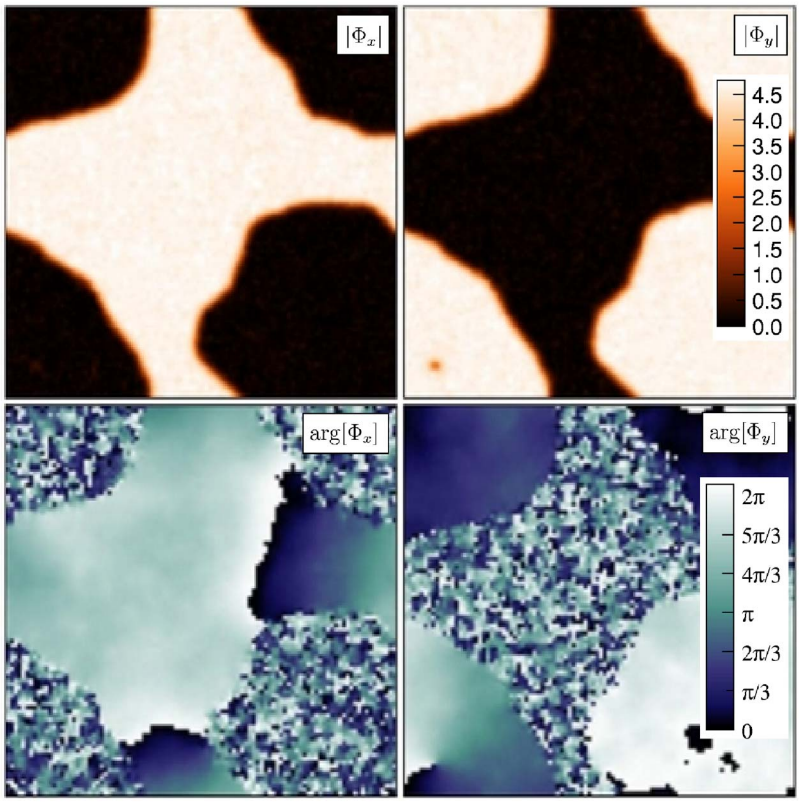

FIG. 4. (Color online) The ground state field configuration on a 100×100 lattice for a random field standard deviation of $h_0=0.6$ and xy interaction $v=0.1$ for a particular realization of disorder. The phase of $\Phi_{x,y}$ fluctuates strongly in regions where its amplitude is suppressed.

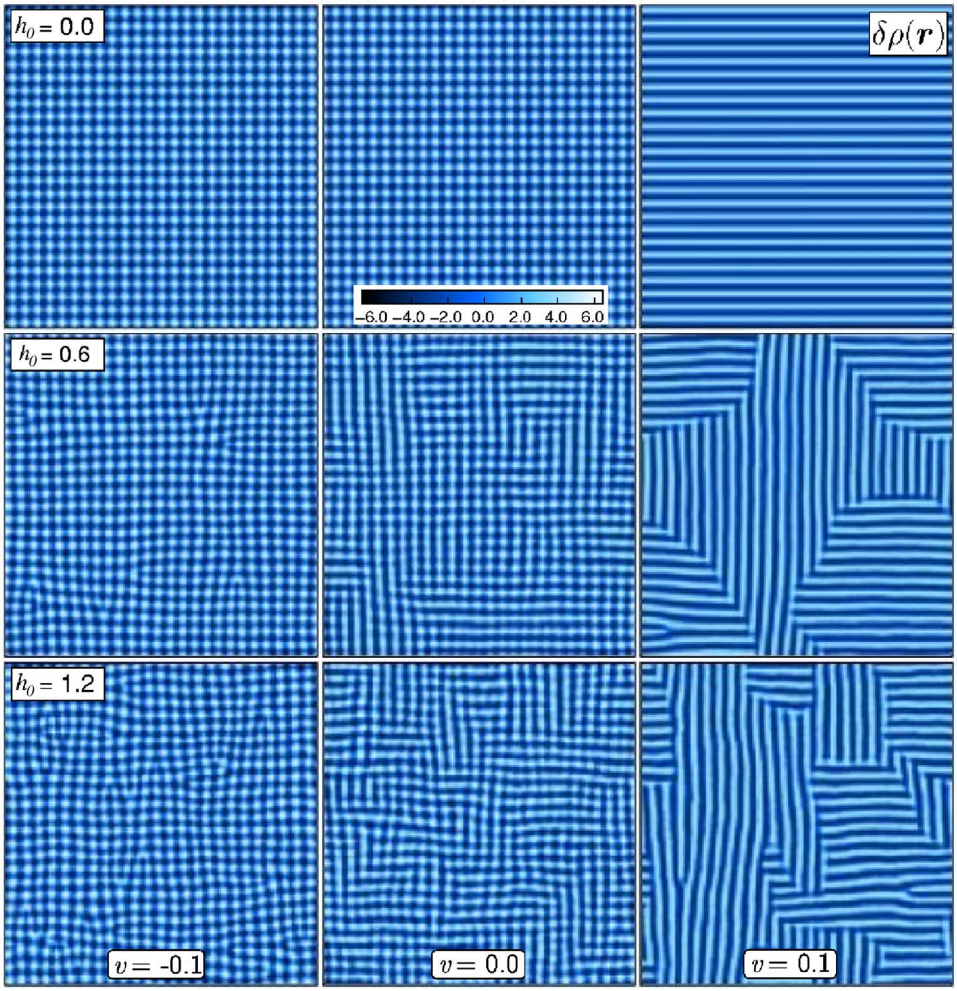

FIG. 5. (Color online) The density fluctuations $\delta\rho(\boldsymbol{r})$ for a CDW period of four lattice spacings ($p=4$) on a 100×100 lattice for $v=-0.1$ (left column), $v=0.0$ (center column), and $v=0.1$ (right column) with $h_0=0.0$, 0.6, and 1.2 from top to bottom for one random field configuration. The central row was constructed using the values of $\Phi_{x,y}$ from Figs. 2–4.

x and y direction have a period of four lattice spacings and identical amplitudes. However, the response of the system to increasing h_0 is very different from the $v=-0.1$ case. For any finite amount of disorder, there is a significant enhancement in the size of unidirectional correlations as the sample breaks up into regions with the magnitude of *either* Φ_x or Φ_y greatly reduced. In the clean limit with $v>0$, we obtain purely unidirectional density fluctuations. As the strength of disorder is increased, large domains of $\pi/2$ relative orientation appear, and finally, for large values of h_0 the system breaks up into many such regions of varying sizes. Qualitative comparison of the central column of Fig. 5 with STM results for the local density of states[1–5] indicates that the correct parameter regime for the model free energy Eq. (2.4) may include moderate disorder ($h_0\simeq0.5$) and a slightly positive value of v.

The presence of such inherent and disorder-induced stripeness leads to the natural definition of a local Ising-like order parameter[22]

$$\Sigma(\boldsymbol{r}) = \frac{|\Phi_x(\boldsymbol{r})|^2 - |\Phi_y(\boldsymbol{r})|^2}{|\Phi_x(\boldsymbol{r})|^2 + |\Phi_y(\boldsymbol{r})|^2}, \tag{4.1}$$

which measures the tendency of the system to have only *one* of either Φ_x or Φ_y nonzero over some finite area, with a value between -1 and 1.

As a result of our direct minimization procedure, we have calculated a full set of low-energy field configurations for multiple system sizes and realizations of disorder with xy couplings $v=\{-0.1,0.0,0.1,0.2\}$ and random field strengths h_0 between 0.0 and 2.0. Using this information, we can construct the disorder-averaged correlation functions for each system size throughout the relevant parameter space. Two distinct types of correlations are of interest. The first are simple CDW correlation functions between the Φ_μ fields given by

$$G_\mu(r) = \overline{\langle \Phi_\mu(r)\Phi_\mu^*(0)\rangle}, \tag{4.2}$$

where $\mu\in\{x,y\}$, whereas the second type measures fluctuations of the Ising-like order parameter Eq. (4.1)

$$G_\Sigma(r) = \overline{\langle \Sigma(r)\Sigma(0)\rangle}, \tag{4.3}$$

with angular brackets indicating a spatial average in the ground state and the overline denotes an average over multiple realizations of disorder $N_{rd}(L)$. As L becomes large both $\langle\Phi_\mu(r)\rangle$ and $\langle\Sigma(r)\rangle$ tend to zero, and the connected and disconnected correlation functions are equivalent. Note that the definition of $G_\Sigma(r)$ distinguishes between regions with strong unidirectional order with $\pi/2$ relative orientation.

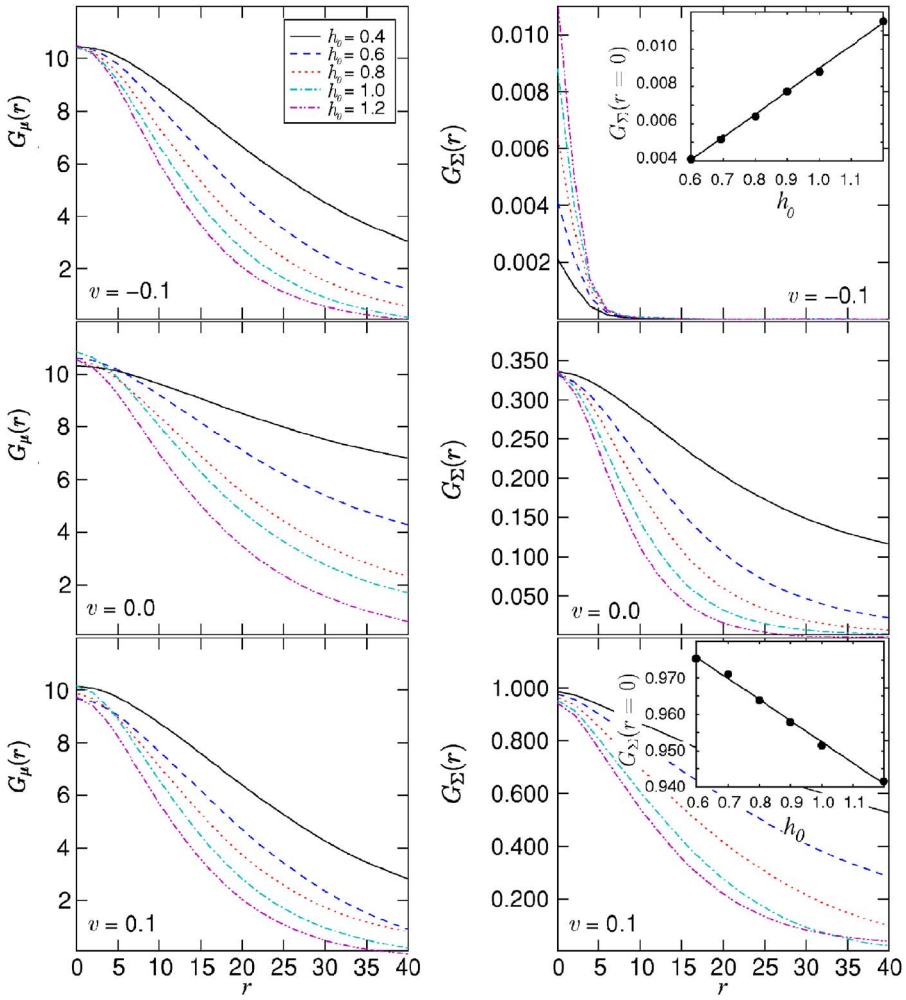

FIG. 6. (Color online) Selected G_μ and G_Σ correlation functions for $v=-0.1, 0.0, 0.1$ and $h_0=0.4, 0.6, 0.8, 1.0, 1.2$ (legend applies to all panels), which were averaged over 100 realizations of disorder in a 100×100 sample. The insets show $\overline{\langle\Sigma^2(0)\rangle}$ vs h_0 for $v=-0.1$ (upper right) and $v=0.1$ (lower right).

For sufficiently large variances in the magnitude of the random field, we expect that both Eqs. (4.2) and (4.3) will be characterized by exponential decays of the form

$$G_\mu(r) \sim e^{-r/\xi_\mu}$$

$$G_\Sigma(r) \sim e^{-r/\xi_\Sigma}, \tag{4.4}$$

where ξ_μ and ξ_Σ are their respective correlation lengths. $G_\mu(r)$ and $G_\Sigma(r)$ are shown for distances up to 40 lattice spacings for $v=-0.1$, 0.0, and 0.1 in Fig. 6.

All correlations appear to decay exponentially for $h_0 \geqslant 0.4$, and the most striking differences between $G_\mu(r)$ and $G_\Sigma(r)$ can be seen at $r=0$ by comparing $\overline{\langle\Phi_\mu^2(0)\rangle}$ and $\overline{\langle\Sigma^2(0)\rangle}$. The xy-interaction parameter v has little effect on the scale of the background CDW order, whereas the background Ising-like order, measured by $G_\Sigma(0)$, increases by three orders of magnitude as v changes from −0.1 to 0.1. In addition, it appears that (after proper finite size scaling) $G_\mu(0)$ is essentially a monotonically decreasing function of h_0 from the checkerboard to stripe parameter regime. The two insets in Fig. 6 clearly show, however, that the slope of $G_\Sigma(0)$ vs h_0 changes from positive to negative near $v=0.0$.

In order to determine the decay constants associated with $G_\mu(r)$ and $G_\Sigma(r)$, we have performed a discrete Fourier transform of the disorder-averaged correlation functions and fit them to a Lorentzian in k-space for each linear system size, xy interaction, and random field strength. The actual correlation length is assumed to be equal to the width of the Lorentzian. Finite size scaling was then performed for each value of v and h_0, as shown for $v=-0.1$ and $h_0=0.6$ in Fig. 7 to extract approximate infinite system size values of ξ_μ and ξ_Σ. The results of the finite size scaling procedure can be seen in Fig. 8 where we plot the decay constants associated with G_x and G_Σ as a function of random field strength h_0 for various values of v, the error bars in the fits are on the order of the symbol sizes.

For a fixed value of v, both ξ_x and ξ_Σ decrease monotonically as a function of disorder strength. The dependence of correlation lengths on the xy coupling v for a fixed random field strength is more interesting, as both correlation lengths are nonmonotonic functions of v. Changing v from −0.1 to 0.0, the correlation length ξ_x increases by almost ten lattice spacings in the regime of moderate disorder strength. This increase can probably be attributed to the fact that for $v=0.0$, our model decomposes into two completely uncoupled unidirectional CDWs with ordering in the x and y direction, respectively. As disorder has a weaker influence on a unidirectional CDW as compared to a checkerboard CDW, this dependence of the correlation length on the value of v is

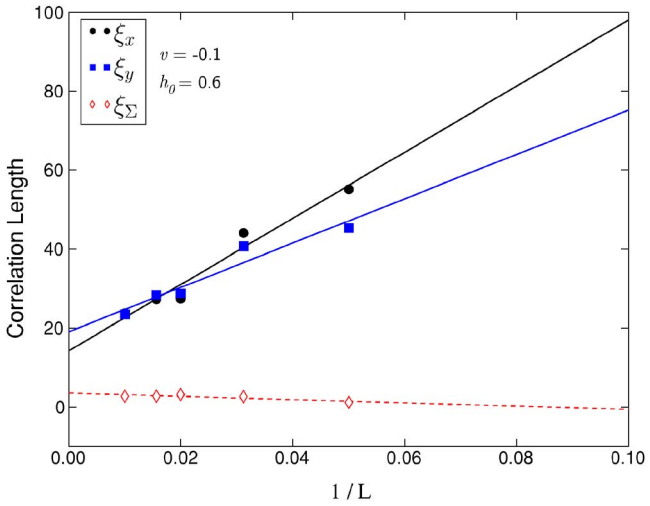

FIG. 7. (Color online) Finite size scaling of the correlation lengths ξ_x, ξ_y, and ξ_Σ using system sizes of $L=\{20,32,48,64,100\}$ for $v=-0.1$ and $h_0=0.6$. y intercepts were extracted to approximate $L\to\infty$.

plausible. A further increase of v to positive values leads to a reduction of ξ_x.

As v controls the degree of stripe order, it is not surprising that the correlation length for the Ising-like order parameter increases from only a few lattice spacings for $v=-0.1$ to 20 to 40 lattice spacings for $v=0.1$ in the regime of moderate disorder strength. It is important to note that for $v=-0.1$ and $v=0.0$, Ising correlations are exclusively due to disorder fluctuations. When v approaches zero coming from negative values, fluctuations of the two fields Φ_x and Φ_y are increasingly independent, and Ising correlations increase. When

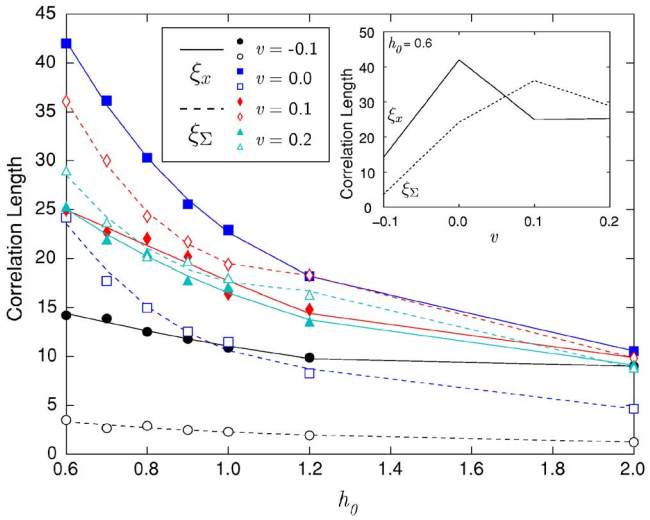

FIG. 8. (Color online) The correlation lengths associated with the exponential decay of $G_x(r)$ and $G_\Sigma(r)$ extracted from finite size scaled Lorentzian widths in Fourier space. Symbol type denotes different values of v; closed symbols with solid lines refer to ξ_x, and open symbols with dashed lines correspond to ξ_Σ. The inset shows the two types of correlation lengths plotted for fixed h_0 as a function of v. Note that the maximum values occur at different values of the xy coupling.

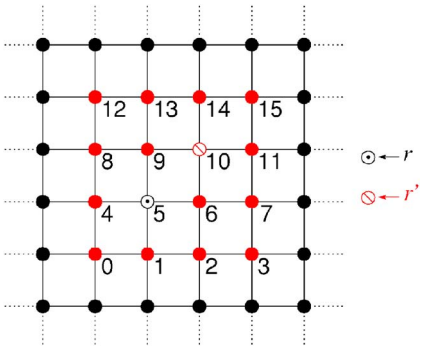

FIG. 9. (Color online) One of N 4×4 boxes used in the calculation of $S_\square(\boldsymbol{r},\boldsymbol{r}'-\boldsymbol{r}'')$. Here, $\square_{\boldsymbol{r}}$ has relative site labels 0 to 15 and is centered at site 5 with $\boldsymbol{r}'$ currently located at site 10.

moving further into the stripe regime, we find $\xi_\Sigma(v=0.1)>\xi_\Sigma(v=0.2)$ for all values of h_0. This can be attributed to the sharpening of domain walls between striped regions with relative orientation $\pi/2$, allowing them to better accommodate the value of the local random field, increasing their overall length.

While ξ_x reaches a maximum value at $v=0$, ξ_Σ peaks at $v=0.1$ (see inset of Fig. 8). The fact that these peaks occur at different values of v leads to the interesting situation that $\xi_\Sigma>\xi_x$ for positive v. Hence, with respect to the analysis of experimental data, $\xi_\Sigma>\xi_x$ is a clear signature for a striped charge order if no random potential was present. In the limit of large v, the system breaks up into domains with either Φ_x or Φ_y order and the correlation lengths ξ_x and ξ_Σ become equal to each other.

V. EMPIRICAL DETERMINATION OF STRIPENESS

In Sec. IV, the analysis of correlation functions exploited our ability to calculate the effective Ising-like order parameter defined in Eq. (4.1) using the ground state values of the independent CDW order parameters $\Phi_{x,y}$. However, we wish to make contact with the STM experiments discussed in Sec. I, which measure the spatial dependence of the local density of states (corresponding to the density fluctuations measured in this study). Therefore, it would be useful to develop a method of analyzing $\delta\rho(\boldsymbol{r})$ directly, which might expose any underlying local Ising-like correlations that are not readily apparent in either real or Fourier space.

With this goal in mind, we propose a method for analyzing experimentally measured STM data on the spatially varying DOS. We begin by defining an effective local Ising-like order parameter $\tilde{\Sigma}(\boldsymbol{r})$ at each of N data points in a LDOS dataset through the following procedure, with more detail provided in the Appendix. (i) Identify the wave vectors $\boldsymbol{K}_x,\boldsymbol{K}_y$, which describe the CDW order, and determine the average number of data points n_p corresponding to a single period in either the x or y direction. In this study, we have fixed $p=4$, $\boldsymbol{K}_\mu=(2\pi/pa)\hat{\mathbf{e}}_\mu$ and only sample data points that are commensurate with the lattice so $n_p=p$. (ii) Surround each data point labeled by $\boldsymbol{r}$ with a $n_p\times n_p$ box $\square_{\mathbf{r}}$ (depicted in Fig. 9), which is "centered" as close to $\boldsymbol{r}$ as possible. (iii)

Define a local density-density correlation function, which lives in each $n_p \times n_p$ box (the smallest that contains enough information to resolve the wave vectors $\{\pm \boldsymbol{K}_x, \pm \boldsymbol{K}_y\}$) that is arbitrarily assigned to the central point. The result is N $n_p \times n_p$ matrices

$$S_{\square}(\boldsymbol{r}, \boldsymbol{r}' - \boldsymbol{r}'') = \langle \delta\rho(\boldsymbol{r}')\, \delta\rho(\boldsymbol{r}'') \rangle_{\boldsymbol{r}' - \boldsymbol{r}'' \in \square_{\boldsymbol{r}}} \tag{5.1}$$

where the right-hand side of Eq. (5.1) indicates an average over all sites $\boldsymbol{r}' \in \square_{\boldsymbol{r}}$ and whose rows and columns are labeled by the x and y components of $\boldsymbol{r}' - \boldsymbol{r}''$ employing periodic boundary conditions for the box. The specific form of one of the matrices contributing to this sum is given in Eq. (A1). (iv) Perform a local discrete Fourier transform of Eq. (5.1) using only those points in $\square_{\boldsymbol{r}}$

$$S_{\square}(\boldsymbol{r}, \boldsymbol{k}) = \frac{1}{n_p^2} \sum_{\boldsymbol{r}' \in \square_{\boldsymbol{r}}} S_{\square}(\boldsymbol{r}, \boldsymbol{r}') e^{-i\boldsymbol{k}\cdot\boldsymbol{r}'} \tag{5.2}$$

for $\boldsymbol{k} \in \{\pm \boldsymbol{K}_x, \pm \boldsymbol{K}_y\}$ at each of the N boxes. (v) Finally, define an effective local Ising-like order parameter as the difference of local structure factor amplitudes at $\pm \boldsymbol{K}_x$ and $\pm \boldsymbol{K}_y$ scaled by their sum inside each box

$$\tilde{\Sigma}(\boldsymbol{r}) = \frac{S_{\square}(\boldsymbol{r}, \boldsymbol{K}_x) + S_{\square}(\boldsymbol{r}, -\boldsymbol{K}_x) - S_{\square}(\boldsymbol{r}, \boldsymbol{K}_y) - S_{\square}(\boldsymbol{r}, -\boldsymbol{K}_y)}{S_{\square}(\boldsymbol{r}, \boldsymbol{K}_x) + S_{\square}(\boldsymbol{r}, -\boldsymbol{K}_x) + S_{\square}(\boldsymbol{r}, \boldsymbol{K}_y) + S_{\square}(\boldsymbol{r}, -\boldsymbol{K}_y)}. \tag{5.3}$$

We may now directly compare Eqs. (4.1) and (5.3) for different values of v at fixed h_0 as seen in Fig. 10. The similarity between $\Sigma(\boldsymbol{r})$ and $\tilde{\Sigma}(\boldsymbol{r})$ is striking and shows both environs of checkerboard order [dark regions, $|\Phi_x(\boldsymbol{r})| = |\Phi_y(\boldsymbol{r})|$] and stripe order [light regions, $|\Phi_x(\boldsymbol{r})| \neq |\Phi_y(\boldsymbol{r})| = 0$].

The agreement between the left and right panels in Fig. 10 can be further quantized by defining an equal point correlator

$$\mathcal{Q} = \frac{\langle \Sigma(\boldsymbol{r}) \tilde{\Sigma}(\boldsymbol{r}) \rangle - \langle \Sigma(\boldsymbol{r}) \rangle \langle \tilde{\Sigma}(\boldsymbol{r}) \rangle}{\sigma_\Sigma \sigma_{\tilde{\Sigma}}}, \tag{5.4}$$

where σ_Σ is the standard deviation of $\Sigma(\boldsymbol{r})$

$$\sigma_\Sigma = \sqrt{\langle \Sigma^2(\boldsymbol{r}) \rangle - \langle \Sigma(\boldsymbol{r}) \rangle^2}. \tag{5.5}$$

Using this definition, we find values for $\mathcal{Q}$ of 0.62, 0.92, and 0.71 for $h_0 = 1.0$ and $v = -0.1$, 0.0, and 0.1. The smaller correlations for $v = \pm 0.1$ are due to the fact that $\square_{\boldsymbol{r}}$ cannot be constructed symmetrically about the site $\boldsymbol{r}$ as we need to resolve the specific wave vectors $\{\pm \boldsymbol{K}_x, \pm \boldsymbol{K}_y\}$, and thus, small regions with rapid changes in $\Phi_{x,y}$ (sharp domain walls) will be poorly reproduced by the effective field $\tilde{\Sigma}$.

A further comparison can be made by examining the disorder-averaged values of the magnitudes of the direct and effective Ising-like order parameters,

$$\overline{|\Sigma|} = \overline{\langle |\Sigma(\boldsymbol{r})| \rangle}$$

$$\overline{|\tilde{\Sigma}|} = \overline{\langle |\tilde{\Sigma}(\boldsymbol{r})| \rangle}, \tag{5.6}$$

which are shown in Fig. 11 for various values of v as a function of disorder. Again we observe significant agreement between the direct and effective Ising-like order parameters,

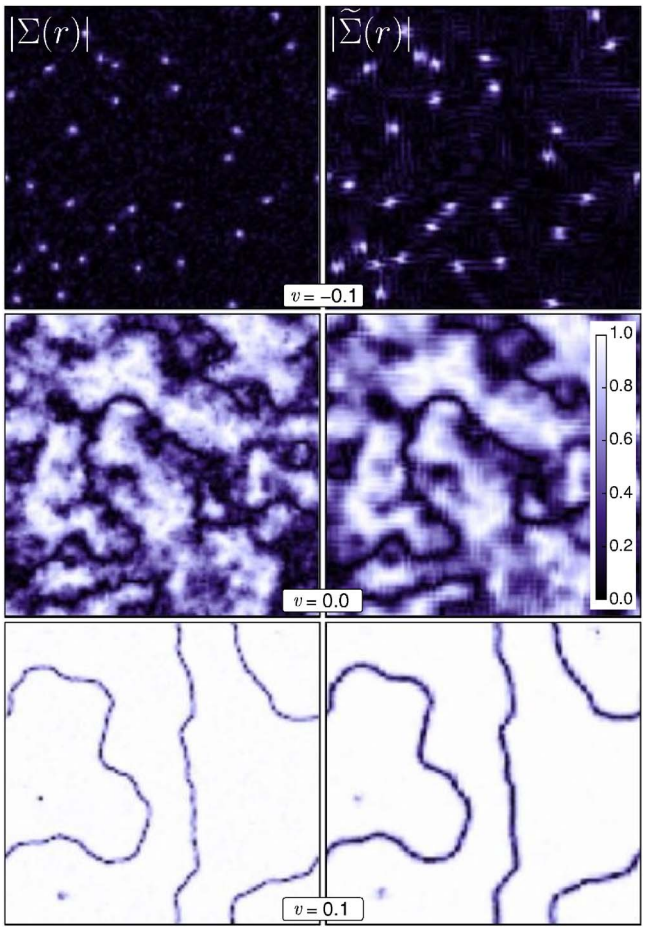

FIG. 10. (Color online) A comparison between the magnitude of the direct (Σ, left-panels) and effective ($\tilde{\Sigma}$, right panels) Ising-like order parameters for $h_0 = 1.0$ and $v = \{-0.1, 0.0, 0.1\}$ for a particular realization of disorder in a 100×100 sample with $n_p = p = 4$.

now having averaged over 100 realizations of disorder. At $h_0 = 0.0$, we recover the results that in the disorder-free theory $\overline{|\tilde{\Sigma}|}$ should be identically zero for $v \leqslant 0$ and equal to one for $v > 0$. Increasing disorder causes a smooth increase in unidirectional order for $v < 0$ and a reduction for $v > 0$ with the effective order parameter having a slightly larger dependence on h_0. For $v = 0.0$, the magnitude of Ising-like order quickly jumps to a value near 0.5.

The concurrence between $\Sigma(\boldsymbol{r})$ and the effective object $\tilde{\Sigma}(\boldsymbol{r})$ inferred from the scaled difference in local structure factor peaks amplitudes at wave vectors $\pm \boldsymbol{K}_x$ and $\pm \boldsymbol{K}_y$ is not surprising in the context that they are both calculated from the same underlying complex fields $\Phi_{x,y}$ in the condensed phase. However, the utility of Eq. (5.3) becomes apparent when considering the plethora of experimental STM spectra where only the LDOS is measured and the underlying order is a topic of hot debate. The current analysis of such spectra involves performing a discrete Fourier transform over the entire field of view. In real materials, disorder plays an important role, and short density-density correlation lengths are often observed. Therefore, such a *global* Fourier transform discards a large amount of relevant local information which could, in principle, be used to probe any hidden electronic structure.

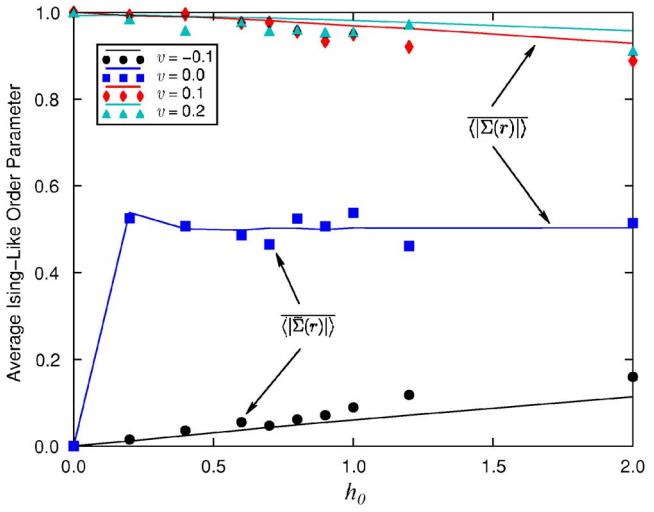

FIG. 11. (Color online) A comparison of the disorder averaged magnitudes of Σ and $\tilde{\Sigma}$ for a 100×100 sample as a function of the variance of the random field. Finite size scaling appears to have little effect on these results. Symbols show the value of $\langle|\tilde{\Sigma}(\boldsymbol{r})|\rangle$ while lines refer to $\overline{\langle|\Sigma(\boldsymbol{r})|\rangle}$.

VI. UNCOUPLED THEORY

In the limit of large disorder a number of results can be explained for the uncoupled theory with $v=0$. On examination of the various correlation lengths in Fig. 8, it is apparent that ξ_x is almost twice as large as ξ_Σ for $v=0$. This can be understood with the help of an approximate analytical argument: for $v=0$, the lattice model Eq. (3.1) reduces to two uncoupled unidirectional CDWs in the x and y directions. Concentrating on the numerator of the Ising order parameter [Eq. (4.1)] for the moment, in the case $v=0$ the correlation function of Σ is then proportional to $\langle|\Phi_x(r)|^2|\Phi_x(0)|^2\rangle$. If fluctuations of Φ_x were described by a simple Gaussian theory, this would imply $\xi_x=2\xi_\Sigma$, which is indeed approximately found in Fig. 8.

A similar approach can be used to account for the saturation of $\overline{|\Sigma|}$ and $|\tilde{\Sigma}|$ to 0.5 for $v=0$ as seen in Fig. 11. Again if we assume uncoupled fluctuations in $\Phi_{x,y}$ described by a normal distribution with mean 0 and variance σ_Φ^2, we can directly calculate the expectation value of Σ by performing integrals in polar coordinates

$$\left\langle \frac{(|\Phi_x|^2-|\Phi_y|^2)^2}{(|\Phi_x|^2+|\Phi_y|^2)^2} \right\rangle = \frac{1}{2}. \tag{6.1}$$

VII. CONCLUSIONS

This paper has characterized the correlations in a disordered CDW state on the square lattice as a function of the parameter v in $\mathcal{F}_\Phi$ (which measures the degree of unidirectionality of the CDW order, $v<0$ corresponding to checkerboard states), and the random field strength h_0. We introduced a number of diagnostics to study the nature of the disordered state: the correlation lengths, ξ_μ, of the CDW order, the correlation length ξ_Σ of the Ising order associated with the unidirectionality, the on-site amplitudes $G_\mu(0)$, $G_\Sigma(0)$, of these orders, and also discussed in Sec. V how closely related quantities could be measured directly in experiments.

Our results are presented in detail in Secs. IV and V, and here we highlight some notable features: (i) As is clear from the insets of Fig. 6, for $v<0$, the strength of the Ising order *increases* with random-field strength, whereas the opposite is true for $v>0$. (ii) The correlation length $\xi_\Sigma>\xi_\mu$ only for $v>0$, and this can serve as a diagnostic for the sign of v in an analysis of the experiments. (iii) We have shown that the correlator $S_\square$ in Eq. (5.1) can serve as a very faithful diagnostic of the structure of Σ, and this should easily enable us to place experimental observations in the appropriate parameter space of the present theory.

A full interpretation of the experiments should include a direct analysis of the experimental data along the lines proposed here. Nevertheless, a comparison of the qualitative structure of the figures presented here (especially Fig. 5) with, e.g., the STM observations of $Ca_{2-x}Na_xCuO_2Cl_2$ by Hanaguri *et al.*[1] does indicate that this system has a value of v close to zero and likely positive.

This would indicate that there exists more prominent unidirectional correlations in the local density of states than what is apparent from a visual inspection of the tunneling spectra alone, especially in the presence of disorder. Such a result is consistent with the emerging picture of universal spin fluctuations measured by neutron scattering in $La_{2-x}Sr_xCuO_4$ and $YBa_2Cu_3O_{6+x}$ thought to be described by models of static or fluctuating stripes.[23]

For the future, our approach offers an avenue to quantitatively correlate the STM experiments with neutron scattering. In particular, after determining the appropriate parameter regime of $\mathcal{F}_\Phi$ from an analysis of the STM data, the resulting $\delta\rho(\boldsymbol{r})$ configurations can be used as an input to determining the dynamic spin structure factor, as discussed in recent works.[24,25]

While this paper was being completed, we learned of related results obtained by Robertson *et al.*[26]

ACKNOWLEDGMENTS

The authors thank L. Bartosch, A. Kapitulnik, S. Kivelson, R. Melko, and in particular J. Hoffman for discussions relating to multiple aspects of this work, and J. Hoffman. In addition, this work benefited from valuable discussions with T. Nattermann. We thank J. Robertson for giving us a preview of their related results.[26] This research was supported by NSF Grant No. DMR-0537077. A.D. acknowledges the National Science and Engineering Council of Canada for financial support through Grant No. PGS D2-316308-2005. B.R. acknowledges support through the Heisenberg program of DFG. The computer simulations were carried out using resources provided by the Harvard Center for Nanoscale Systems, part of the National Nanotechnology Infrastructure Network.

APPENDIX: LOCAL ISING-LIKE ORDER PARAMETER

This appendix provides more detail on the method used in the calculation of the effective local Ising-like order parameter $\tilde{\Sigma}(\boldsymbol{r})$ described in Sec. V for the specific case of $n_p=p=4$. Consider Fig. 9, which shows one of N 4×4 boxes $\square_{\boldsymbol{r}}$, where the sites contained within the box are given the relative labels 0–15 and it is "centered" at the (1,1) point here labeled 5.

For the particular case shown in Fig. 9 with $\boldsymbol{r}'=\boldsymbol{r}'_{10}$, one of the 16 matrices that contributes to the average $S_{\square}(\boldsymbol{r},\boldsymbol{r}'-\boldsymbol{r}'')$ in Eq. (5.1) is written out explicitly as

$$S_{\square}(\boldsymbol{r},\boldsymbol{r}'-\boldsymbol{r}'')=\cdots+\frac{\delta\rho(\boldsymbol{r}'_{10})}{16}\begin{pmatrix}\delta\rho_{14}+\delta\rho_6 & \delta\rho_5+\delta\rho_7+\delta\rho_{13}+\delta\rho_{15} & 2(\delta\rho_4+\delta\rho_{12}) & \delta\rho_5+\delta\rho_7+\delta\rho_{13}+\delta\rho_{15}\\ 2\delta\rho_2 & 2(\delta\rho_1+\delta\rho_3) & 4\delta\rho_0 & 2(\delta\rho_1+\delta\rho_3)\\ \delta\rho_{14}+\delta\rho_6 & \delta\rho_5+\delta\rho_7+\delta\rho_{13}+\delta\rho_{15} & 2(\delta\rho_4+\delta\rho_{12}) & \delta\rho_5+\delta\rho_7+\delta\rho_{13}+\delta\rho_{15}\\ \delta\rho_{10} & \delta\rho_9+\delta\rho_{11} & 2\delta\rho_8 & \delta\rho_9+\delta\rho_{11}\end{pmatrix}+\cdots, \tag{A1}$$

where we have employed the shorthand notation $\delta\rho_i\equiv\delta\rho(\boldsymbol{r}''_i)$. After performing the average over all $\boldsymbol{r}'-\boldsymbol{r}''\in\square_{\boldsymbol{r}}$, i.e., calculating all 16 matrices at each site, $S_{\square}(\boldsymbol{r},\boldsymbol{r}'-\boldsymbol{r}'')$ is Fourier transformed over the relative coordinates in the box using Eq. (5.2) to give $S_{\square}(\boldsymbol{r},\boldsymbol{k})$. This expression may then be evaluated at $\pm\boldsymbol{K}_x$ and $\pm\boldsymbol{K}_y$ using Eq. (5.3) to give the effective Ising-like order parameter $\tilde{\Sigma}(\boldsymbol{r})$.

*On leave from the Institut für Theoretische Physik, Universität zu Köln, D-50923, Germany.

[1] T. Hanaguri, C. Lupien, Y. Kohsaka, D.-H. Lee, M. Azuma, M. Takano, H. Takagi, and J. C. Davis, Nature (London) **430**, 1001 (2004).
[2] A. Fang, C. Howald, N. Kaneko, M. Greven, and A. Kapitulnik, Phys. Rev. B **70**, 214514 (2004).
[3] M. Vershinin, S. Misra, S. Ono, Y. Abe, Y. Ando, and A. Yazdani, Science **303**, 1995 (2004).
[4] K. McElroy, D.-H. Lee, J. E. Hoffman, K. M. Lang, J. Lee, E. W. Hudson, H. Eisaki, S. Uchida, and J. C. Davis, Phys. Rev. Lett. **94**, 197005 (2005).
[5] A. Hashimoto, N. Momono, M. Oda, and M. Ido, cond-mat/0512496 (unpublished).
[6] J. M. Tranquada, J. D. Axe, N. Ichikawa, A. R. Moodenbaugh, Y. Nakamura, and S. Uchida, Phys. Rev. Lett. **78**, 338 (1997).
[7] Y. S. Lee, R. J. Birgeneau, M. A. Kastner, Y. Endoh, S. Wakimoto, K. Yamada, R. W. Erwin, S. H. Lee, and G. Shirane, Phys. Rev. B **60**, 3643 (1999).
[8] J. M. Tranquada, H. Woo, T. G. Perring, H. Goka, G. D. Gu, G. Xu, M. Fujita, and K. Yamada, Nature (London) **429**, 534 (2004).
[9] P. Abbamonte, A. Rusydi, S. Smadici, G. D. Gu, G. A. Sawatzky, and D. L. Feng, Nat. Phys. **1**, 155 (2005).
[10] *Spin Glasses and Random Fields*, edited by A. P. Young (World Scientific, Singapore, 1997).
[11] T. Nattermann, Phys. Rev. Lett. **64**, 2454 (1990).
[12] T. Giamarchi and P. Le Doussal, Phys. Rev. B **52**, 1242 (1995).
[13] C. Zeng, P. L. Leath, and D. S. Fisher, Phys. Rev. Lett. **82**, 1935 (1999).
[14] T. Nattermann and S. Scheidl, Adv. Phys. **49**, 607 (2000).
[15] A. Del Maestro and S. Sachdev, Phys. Rev. B **71**, 184511 (2005).
[16] S. Bogner and S. Scheidl, Phys. Rev. B **64**, 054517 (2001).
[17] M. Weigel and M. J. P. Gingras, Phys. Rev. Lett. **96**, 097206 (2006).
[18] S. Kirkpatrick, C. D. Gelatt, and M. P. Vecchi, Science **220**, 671 (1983).
[19] J. R. Shewchuk, *An Introduction to the Conjugate Gradient Method Without the Agonizing Pain* (unpublished).
[20] P. Siarry, G. Berthiau, F. Durbin, and J. Haussy, ACM Trans. Math. Softw. **23**, 209 (1997).
[21] M. J. P. Gingras and D. A. Huse, Phys. Rev. B **53**, 15193 (1996).
[22] S. A. Kivelson, E. Fradkin, V. Oganesyan, I. Bindloss, J. Tranquada, A. Kapitulnik, and C. Howald, Rev. Mod. Phys. **75**, 1201 (2003).
[23] J. M. Tranquada, H. Woo, T. G. Perring, H. Goka, G. D. Gu, G. Xu, M. Fujita, and K. Yamada, Nature (London) **429**, 534 (2004).
[24] M. Vojta and S. Sachdev, J. Phys. Chem. Solids **67**, 11 (2006).
[25] M. Vojta, T. Vojta, and R. K. Kaul, cond-mat/0510448 (unpublished).
[26] J. Robertson, S. A. Kivelson, E. Fradkin, A. Fang, and A. Kapitulnik, cond-mat/0602675 (unpublished).